SEVENTH WORKSHOP ON RESEARCH IN TURBULENCE AND TRANSITION

Escola Tècnica Superior d'Enginyeries Industrial i Aeronàutica de Terrassa

Technical University of Catalonia

Terrassa, October 14th, 2013

Iberian-East ERCOFTAC Pilot Centre

Foreword

The Seventh Workshop on Research in Turbulence and Transition will be held at ETSEIAT (Terrassa School of Industrial and Aeronautical Engineering), in Terrassa (Barcelona, Spain) on October 14th, 2013. These Workshops have been conducted since 2003 at the initiative of CIMNE, Iberian-East and Iberian-West Pilot Centres of the European Research Community on Flow, Turbulence and Combustion (ERCOFTAC), and is a Europe-wide organization that promotes research on topics related to fluid dynamics, turbulence and combustion, and their industrial applications.

The aim of this Workshop is to contribute to a better knowledge of the activities carried out by various Iberian research groups in any field relevant to the turbulence or/and transition. The papers presented correspond to groups from Barcelona, Terrassa and Tarragona.

The organizers of the Workshop want to thank the ETSEIAT at Technical University of Catalonia.

How to arrive

Terrassa School of Industrial and Aeronautical Engineering
Terrassa Campus, Building TR5. C. Colom, 11 08222 Terrassa
http://www.etseiat.upc.edu/contact

10:20	**Welcome**
10:40	**Numerical simulation of heat transfer and temperature distribution in a printed circuit board enclosure** S. Varela, G. Usera, A. Vernet and J.A. Ferrè
11:00	**Analysis of a confined laminar reactive flow in a cylindrical cavity using PLIF and PIV** I. Sancho, s. Varela, J. Pallarés and A. Vernet
11:20	**Analysis of the suction chamber of external gear pumps and their influence on cavitation and volumetric efficiency** D. del Campo, R. Castilla and E. Codina
11:40	**Coffee break**
12:00	**Direct numerical simulation of bubbles rising through viscous liquids** J. Castro, N. Balcázar, l. Jofre, O. Lehmkuhl, J. Rigola, A.Oliva
12:20	**Direct numerical simulation of a NACA0012 airfoil with massive separation** I. Rodríguez, O. Lehmkuhl, R. Borrell, A.Oliva
12:40	**New differential operators and discretization methods for eddy-viscosity models for LES** F. Xavier Trias, A. Gorobets and A. Oliva
13:00	**On the large-eddy simulations of the flow past a cylinder at critical Reynolds numbers** O. Lehmkuhl, I. Rodríguez, J. Chiva and R. Borrell
13:20	**Turbulent jets in iron casting** R. Castilla, G. Raush, E. Dalmau, D. del Campo, E. Codina
13:40	**Lunch**
15:20	**Transient and dynamic numerical simulation of the fluid flow through valves based on large eddy simulation models** J. Rigola, O. Estruch, O. Lehmkuhl, A.Oliva and C.D. Pérez-Segarra
15:40	**Large eddy simulation of a turbulent jet diffusion flame using unstructured meshes** C.D. Pérez-Segarra, J. Ventosa, O. Lehmkuhl and A. Oliva
16:00	**Coffee break**
16:20	**Variational multiscale large eddy simulation of turbulent incompressible flows** O. Colomés, S. Badia, R. Codina and J. Principe
16:40	**Variational multiscale large eddy simulation of turbulent thermally coupled flows** M. Ávila, R. Codina, and J. Principe
17:00	**Final discussion and conclusions**

Numerical simulation of heat transfer and temperature distribution in a Printed Circuit Board enclosure

S. Varela[a], G. Usera[b], A. Vernet[a] and J.A. Ferrè[a]

[a] Departament d'Enginyeria Mecànica, Universitat Rovira i Virgili, Av. Països Catalans 26, 43007, Tarragona, Spain

b Instituto de Mecánica de los Fluidos, Facultad de Ingeniería, Universidad de la República, J.H. Reissig 565, 11300, Montevideo, Uruguay

ABSTRACT

The heat transfer analysis and temperature distribution inside Printed Circuit Board (PCB) enclosures for different geometries was investigated. Herein, the computational fluid dynamic (CFD) solver *caffa3d.MB* [1] was employed to simulate the 3D incompressible Navier-Stokes equations. The numerical method uses a spatial discretization based on block-structured, non-orthogonal body fitted grids. Numerical simulations for two different PCB geometry configurations are analyzed using eight Reynolds numbers. The temperature field is practically the same above the plate encasing the PCB, differences appear below the plate. While analyzing the plane just below for the open geometry the main consideration is the presence of a hot zone. The greater heat transfer is obtained in the top channel for both geometries. In turn in the bottom channel the heat transfer is greater in the closed geometry than the open one. The calculating results show that the cooling of the PCB is more efficient for the closed geometry.

REFERENCES

[1] G. Usera, A. Vernet, J.A. Ferrè, Use of time resolved PIV for validating LES/DNS of the turbulent flow within a PCB enclosure model, Flow Turbulent Combust. 77 (2006) 77-95.

Analysis of a confined laminar reactive flow in a cylindrical cavity using PLIF and PIV

Sancho. I, Varela. S, Pallares. J and Vernet. A
Department of Mechanical Engineering. University Rovira i Virgili
Av. Països Catalans, 26 43007-Tarragona. Spain
Ph. +34 977 558 451, e-mail: irene.sancho@urv.cat

ABSTRACT

In the last years, the studies of macro- and micromixing have advanced to determine where and in which degree these two mixing scales are present in a chemical reaction and therefore improve its throughput. Most of the studies apply the PLIF (Planar Laser Induced Fluorescence) and PIV (Particle Image Velocimetry) techniques to quantify, respectively, the degree of mixing and the concentration fields, and the velocity fields in reactive and non-reactive flows [1,2]. The great majority of authors perform their studies, experimental and computational, in turbulent regime. The comparison of experimental and computational results in turbulent flows is not trivial.

Confined flows show a great interest both in basic research and on diverse technological applications. Over the years, the cylindrical lid-driven cavities have been extensively studied; indeed the flow behaviour has been totally characterized [3], varying the velocity of rotating end wall and the aspect ratio. Even though the velocity fields and the formation of vortices have been studied applying the PIV technique [4].

The aim of this study is to analyse an axisymmetric confined, reactive and laminar flow in a cylindrical cavity with a rotating end wall varying its aspect ratio and the angular velocity of the rotating wall, experimentally, applying simultaneously the PIV and PLIF techniques, and computationally. The lack of information of confined, reactive and laminar flows make this study interesting, taking into account that even it is a laminar flow there are breakdowns keeping the steady state of the flow [3]. Moreover, the laminar flow allows a less complex comparison between the experimental and computational results than in turbulent flow, making the characterisation of the PIV and PLIF techniques possible. Finally, the cylindrical lid-driven cavity study, which has the flow behaviour characterized, enables us focus in the topic that actually we are interested; the degree of mixing in a chemical reaction.

The experimental technique is based on the combined PIV and PLIF system. PIV is applied to measure the instantaneous velocity fields and PLIF is applied to measure the instantaneous concentration. Figure 1 shows a schematic sketch of the experimental setup.

The experimental setup consists of a PMMA cylindrical container of inner radius R=0.04 m with a rotating wall at the top (Fig. 1). The rotating wall is driven by an electronically controlled DC motor, operating with angular velocity between ω=6.25-14.38 rad/s. The height (H) of the flow domain, and therefore the aspect ratio (H/R) can be varied. In this work, three different aspect ratios H/R: 1, 1.5 and 2 were considered. In this case, the traditional lid-driven has been modified introducing an inlet in the center of the bottom wall with an inner diameter of 3 mm, where one of the reactants is released inside the cylindrical cavity.

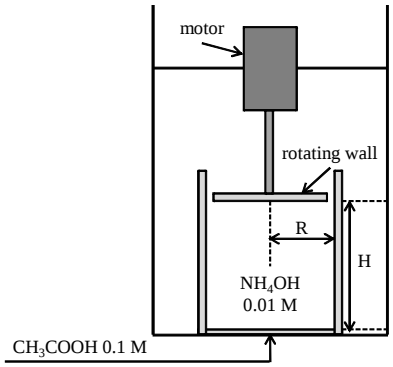

Figure 1 Sketch of experimental setup.

The chemical reaction considered is a neutralization acid-base reaction, i.e:

$$CH_3COOH + NH_4OH \rightarrow CH_3COONH_4 + H_2O$$

This is a rapid irreversible second-order reaction. The reaction rate constant is in the order of 10^8 m^3/mol·s and the concentration of the Acetic Acid (A) and Ammonium Hydroxide (B) are, respectively, 0.1 M and 0.01 M.

The base solution is inside the cylindrical cavity. The acid solution is released inside the cavity by the bottom inlet with the help of a pump. The fluorescent dye (Sodium Fluorescein) is added to the acid with a concentration of 0.08 g/l. The velocity inlet of the acid solution is between v_i =1.6-3.2 mm/s. These velocities are between 50 and 100 times less than the average velocity of the rotating top wall and do not affect the velocity fields of the cylindrical cavity.

The preliminary numerical results are computed for an aspect ratio and a velocity inlet of H/R=2 and v_i=3.2 mm/s, respectively. Figure 2 shows the cross-stream velocity vectors fields at x=0 for different angular velocity of rotating wall. These angular velocities correspond to a Reynolds number (Re) between 1000 and 2300 ($\mathrm{Re} = \omega R^2/\nu$). As indicated by Escudier [3], with a H/R=2 and Re=1500, a breakdown can be observed (Fig. 2b). Figures 2c and 2d show two breakdowns. Figure 3 shows the contours of concentration of the base solution (B) at different reaction time (t). The acid solution enters to cavity up to t=15 min (Fig. 3c), when the half of acid solution volume has entered. The base solution is in excess. Figure 3d shows the consumption of reactive B, that is slowly disappearing. It can be observed that the contours of concentration of base solution have butterfly wings shape during the reaction.

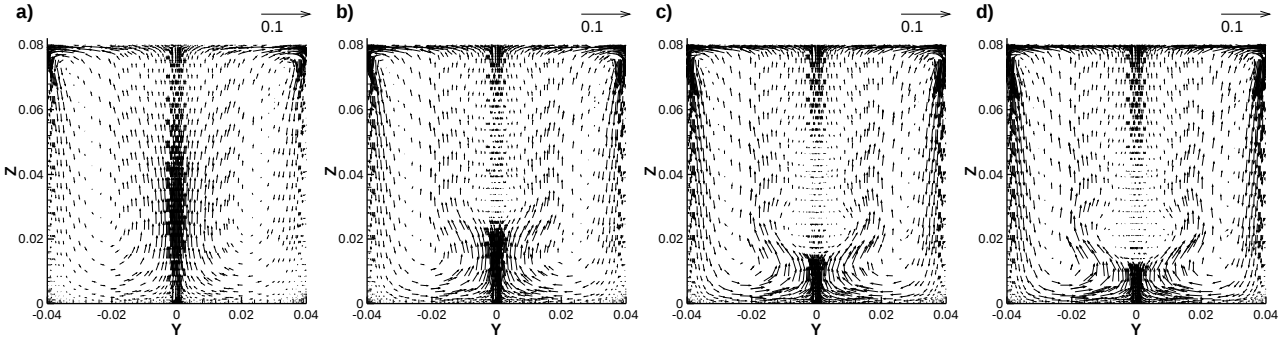

Figure 2 Cross-stream velocity vectors fields at x=0 for (a) ω=6.25 rad/s (Re=1000), (b) ω=9.38 rad/s (Re=1500), (c) ω=12.5 rad/s (Re=2000) and (d) ω=14.38 rad/s (Re=2300).

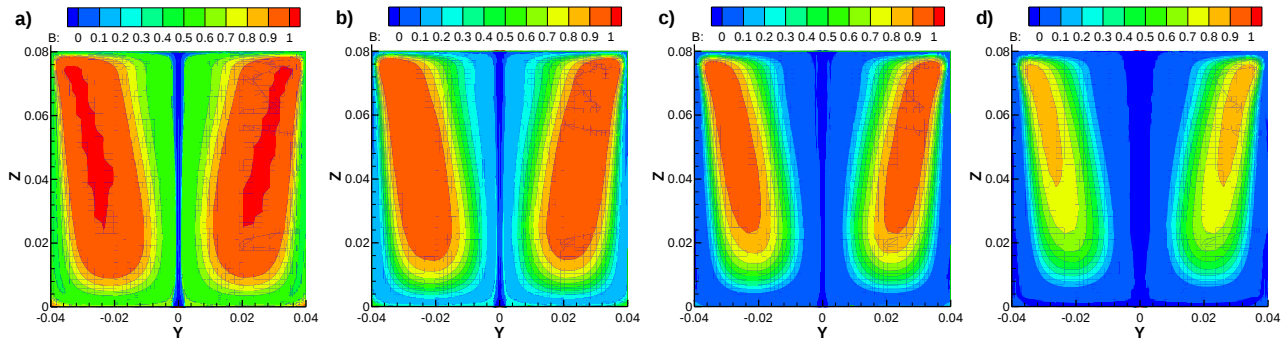

Figure 3 Contours of concentration of base solution at x=0 and ω=6.25 rad/s (Re=1000). (a) t=5 min, (b) t=10 min, (c) t=15 min and (d) t=20 min.

A detailed experimental and computational analysis of the mixing degree and the velocity and concentration fields of the confined, laminar and reactive flow in a cylindrical lid-driven cavity will be included in the final version of the paper varying the aspect ratio and the angular velocity of the container.

REFERENCES

[1] L. K. Hjertager Osenbroch, B. H. Hjertager, and T. Solberg, "Experiments and CFD modelling of fast chemical reaction in turbulent liquid flows," *International Journal of Chemical Reactor Engineering*, vol. 3, 1–30, 2005.

[2] V. Zhdanov and A. Chorny, "Development of macro- and micromixing in confined flows of reactive fluids," *International Journal of Heat and Mass Transfer*, vol. 54, 15–16, 3245–3255, 2011.

[3] M. P. Escudier, "Observations of the flow produced in a cylindrical container by a rotating endwall," *Experiments in Fluids*, vol. 2, 4, 189–196, 1984.

[4] C. Cabeza, G. Sarasúa, A. C. Martí, I. Bove, S. Varela, G. Usera, and A. Vernet, "Influence of coaxial cylinders on the vortex breakdown in a closed flow," *European Journal of Mechanics - B/Fluids*, vol. 29, 3, 201–207, 2010.

Analysis of the suction chamber of external gear pumps and their influence on cavitation and volumetric efficiency

D. del Campo[a], R. Castilla[b] and E. Codina[b]

[a] ETSEIAT – Department of Aeronautics. Politechnical University of Catalonia.
[b] LABSON - Department of Fluid Mechanics. Politechnical University of Catalonia.

ABSTRACT

Hydraulic machines are faced with increasingly severe performance requirements. The need to design smaller and more powerful machines rotating at higher speeds in order to provide increasing efficiencies has to face a major limitation: cavitation.

A two-dimensional numerical approach, by means of Computational Fluid Dynamics (CFD), has been developed for studying the effect of cavitation in the volumetric efficiency of external gear pumps. Several cavitation models and grid deformation algorithms have been studied, and a method for simulating the contact between solid boundaries has been developed. The velocity field in the inlet chamber has also been experimentally measured by means of Time-Resolved Particle Image Velocimetry (TRPIV) and results have been compared to the numerical ones in order to validate the accuracy of the model.

Our two-dimensional model is not able to predict the real volumetric efficiency of the pump, since several simplifications are involved in it. Nevertheless, this model shows to be valid to understand the complex flow patterns that take place inside the pump and to study the influence of cavitation on volumetric efficiency. The influence of the rotational speed of the pump has been analyzed, as well as the effect the working pressure.

DIRECT NUMERICAL SIMULATION OF BUBBLES RISING THROUGH VISCOUS LIQUIDS

J. Castro[1], N. Balcázar[1], L. Jofre[1], O. Lehmkuhl[1,2], J. Rigola[1], A.Oliva[1]
[1]Centre Tecnològic de Transferència de Calor (CTTC), Universitat Politècnica de Catalunya (UPC), Spain
[2] Termo Fluids S.L., Spain

INTRODUCTION

Gravity-driven bubbly flow is a complex phenomenon which is difficult to understand, predict and model. The modelling of averaged properties of two-phase flows has traditionally suffered from the lack of detailed and reliable data against which closure models can be validated. Direct Numerical Simulations (DNS) of multiphase flows by interface tracking techniques have now advanced to the point that they are able to provide such data for bubbly flow systems.

In this work, a numerical method is introduced for DNS of bubbly flows, which is integrated in a finite-volume framework on collocated unstructured grids of arbitrary element type. The location, geometry and the movement of the discontinuities are described by the conservative level-set method (CLS). The CLS method is validated with experimental results of the bouyant rise of an isolated bubble, and finally the method is applied to simulate the gravity-driven bubbly flow. In general, a good agreement is found between the current simulations and results reported in the literature.

DESCRIPTION OF NUMERICAL METHOD

The conservation of momentum and mass of two immiscible incompressible fluids are described by the Navier-Stokes equations:

$$\begin{cases} \frac{\partial}{\partial t}(\rho\mathbf{v}) + \nabla\cdot(\rho\mathbf{v}\mathbf{v}) = -\nabla p + \nabla\cdot\mu\left(\nabla\mathbf{v} + (\nabla\mathbf{v})^T\right) + \rho\mathbf{g} + \sigma\kappa\delta_\Gamma\mathbf{n}, \\ \beta = \beta_1 H_\Gamma + \beta_2(1-H_\Gamma) \qquad \text{with } \beta \in \{\rho,\mu\}. \end{cases} \tag{1}$$

$$\nabla\cdot\mathbf{v} = 0 \tag{2}$$

where ρ and μ denote the density and dynamic viscosity of the fluids, $\mathbf{v}$ is the velocity field, $\mathbf{g}$ is the gravity acceleration, p is the pressure, σ is the coefficient of surface tension, $\mathbf{n}$ is the interface normal, κ is the interface curvature, δ_Γ and H_Γ are the Dirac delta function and Heaviside step function localized at the interface, $\Gamma(t)$.

In the conservative level-set method (CLS) [2] a regularized indicator function is used for interface capturing:

$$\phi(\mathbf{x},t) = \frac{1}{2}\left(tanh\left(\frac{d(\mathbf{x},t)}{2\varepsilon}\right)+1\right) \tag{3}$$

where $d(\mathbf{x},t) = sign(\mathbf{x},t)min\{||\mathbf{x}-\mathbf{x}_\Gamma(t)||\}$ is a signed distance function, $\mathbf{x}_\Gamma \in \Gamma$, ε is a parameter that sets the thickness of the profile, ϕ takes the value 0 in one fluid and the value 1 in the other fluid. The interface, Γ, is defined by the location of the $\phi = 0.5$ iso-surface. The interface transport equation can be written in conservative form provided the velocity field is solenoidal:

$$\frac{\partial\phi}{\partial t} + \nabla\cdot\phi\mathbf{v} = 0 \tag{4}$$

Furthermore, an additional re-initialization equation is introduced to keep the profile and thickness of the interface constant,

$$\frac{\partial\phi}{\partial\tau} + \nabla\cdot\phi(1-\phi)\mathbf{n}_{\tau=0} = \nabla\cdot\varepsilon\nabla\phi \tag{5}$$

This equation is advanced in pseudo-time τ, it consists of a compressive flux $\phi(1-\phi)\mathbf{n}_{\tau=0}$ that aims at sharpening the profile, and of a diffusion term $\nabla\cdot\varepsilon\nabla\phi$ that ensure the profile remains of characteristic thickness ε. Geometrical information on the interface ($\mathbf{n}$ and κ) is obtained through:

$$\mathbf{n} = \frac{\nabla\phi}{\|\nabla\phi\|} \qquad \kappa(\phi) = -\nabla\cdot\mathbf{n} \tag{6}$$

In order to avoid the appearance of numerical instabilities near the interface, surface tension force is smoothed over a finite thickness by using the CSF model [1], $\sigma\kappa\mathbf{n}\delta_\Gamma = \sigma\kappa\nabla\phi$, and fluid properties are regularized by the level-set function ϕ, $\beta(\phi) = \beta_1\phi + \beta_2(1-\phi)$.

The governing equations have been discretised on a collocated unstructured grid arrangement by means of the finite-volume method. To avoid unphysical oscillations in the level set function, a TVD Superbee limiter, is used to discretize the convective term in advection Eq. (4). Central difference scheme, is used to discretize both the convective and compressive terms of momemtum Eq. (1) and re-initialization Eq. (5) respectively. The velocity-pressure coupling has been solved by means of a classical fractional step projection method. For the temporal discretization, explicit Adams-Bashforth scheme is used for the momemtum equation, while for the pressure-gradient term an explicit first-order scheme has been used. Advection Eq. (4) and Re-initialization Eq. (5) are integrated in time with a 3-step third-order accurate TVD Runge-Kutta method.

RESULTS

To validate the numerical method, the bouyant rise of a single bubble is first simulated. For bubbles rising freely in infinite media a generalized graphical correlation is given by Grace [4]. This diagram shows the shape regimes and terminal velocities in terms of Eötvös number $Eo = gd^2\Delta\rho/\sigma$, Morton number $M = g\mu_1^4\Delta\rho/(\rho_1^2\sigma^3)$ and Reynolds number $Re = \rho_1 U_T d/\mu_1$. Here, U_T is used to denote the terminal velocity of the bubble, $\Delta\rho = \rho_1 - \rho_2$ specifies the density difference between the fluid phases, the subscript 1 refers to the heavier fluid and the subscript 2 to the lighter fluid.

Computational domain consists of a cylinder of diameter $D = 6d$ and height $H = 8d$, where d is the initial diameter of the bubble. Initially the spherical bubble is located on the symmetric axis at distance d from the bottom wall. Both liquid and bubble are assumed initially quiescent. No-slip boundary conditions are applied on top, side and bottom walls.

The density and viscosity ratios are specified respectively as $\rho_1/\rho_2 = 100$ and $\mu_1/\mu_2 = 100$. The time step size is fixed to $\Delta t^* = 5.0\times 10^{-5}$ ($t^* = t(g/d)^{1/2}$). An interface thickness parameter, $\varepsilon = 0.5h^{0.9}$, is used in all simulations of this work, where h is the characteristic grid size. In the numerical experiments we have observed that $25cv/d$ is enough for accurate capturing of shape and terminal velocity of the bubbles. Hence, the computational domain has been discretized by 2.3 million control volumes, with a grid densified around the symmetry axis of the cylinder to maximize the bubble resolution ($25cv/d$).

Numerical results for various values of Eo number and M number are shown in Fig. 1. The dimensionless numbers reported here are evaluated at the initial stage using the droplet diameter d. From the simulations presented in Fig. (1), it can be concluded the current numerical method is robust enough to predict the various bubble shapes under a wide range of flow regimes. The comparison of the terminal Reynolds numbers for the experiment and simulation cases is listed in Table 1. The results from simulations agree with those of experiments very well.

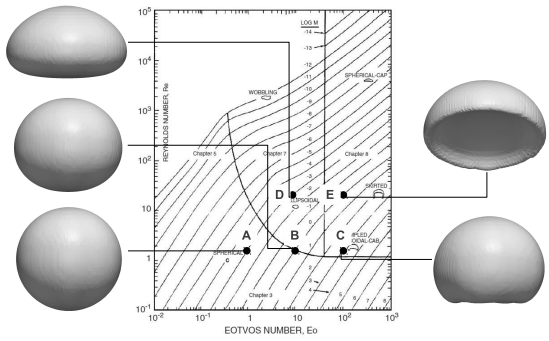

Figure 1: Bubble diagram of Grace for the shape and terminal velocities of gas bubbles in quiescent viscous liquids, reproduced from Clift et al. (1978) [4]. The simulated cases are indicated with capitals.

Bubble regime	M	Eo	Re_G	Re_C	Case
Spherical	1.26×10^{-3}	1.0	1.7	1.68	**A**
Ellipsoidal	1.00×10^{0}	10.0	1.7	1.75	**B**
Ellipsoidal Cap.	1.00×10^{3}	97.1	1.5	1.58	**C**
Ellipsoidal	9.71×10^{-4}	10.0	22.0	23.0	**D**
Skirted	9.71×10^{-1}	97.1	20.0	18.7	**E**

Table 1: Simulation of rising bubble for different regimes according to the bubble diagram of Grace [4]. Re_G represents the experimental Reynolds number obtained from the Grace diagram and Re_C represents the predicted Reynolds number.

The oblique coalescence of two rising bubbles in an initially quiescent liquid is explored. Numerical parameters are the same as in previous cases. A sequence of shapes for coalescence process of two bubbles is presented in Fig. 3. Bubbles start to rise due to buoyancy, subsequently, a vortice is created in the wake of the upper bubble. The suction by the top bubble produce the collision between them and the thin liquid film between the bubbles is squeezed out and ruptured. Finally, the two bubbles merge into a single bubble, completing the coalescence process. The numerical prediction match faily well in terms of bubble shapes with the experimental results reported by Brereton and Korotney [5].

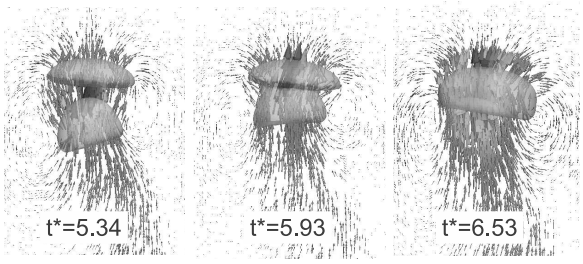

Figure 2: Oblique bubble coalescence of two initially spherical bubbles. Here $M = 0.0002$, $Eo = 16$, $\rho_1/\rho_2 = 100$, $\mu_1/\mu_2 = 100$.

With the confidence from validating the CLS method, the model is used to explore the gravity-driven bubbly flow. A set of 30 rising bubbles with the same diameter d is simulated in a cylindrical duct, for $\rho_1/\rho_2 = 10$, $\mu_1/\mu_2 = 10$, $Eo = 2.25$ and $M = 6\times10^{-4}$. Bubbles are initially placed in the domain in a random pattern. The volume fraction occupied by bubbles in the whole domain is 0.034%, and the minimal distance between the bubbles at initial state is $1.25d$. Computational domain is discretized by 12.6×10^{6} $cv \equiv 30cv/d$. The simulation results are performed by using a time step $\Delta t^* = 2.0\times10^{-4}$. Periodic boundary condition is applied at the top and bottom of the domain, whereas no-slip boundary condition is applied at the side wall.

Fig. 3 shows the pattern of bubbly flow. Bubbles rise due the bouyancy force, and form its own wake. The dynamic interaction process of bubbles is dominated by wake effects. A bubble moving in the wake of another bubble is attracted toward the leading bubble. The strength of influence depends of distance between bubbles. Coalescence processes are observed as the time is increased, and large bubbles are formed, which then induces a stronger flow field that affect the neighbor bubbles. The bubbles in this regime flow moves through the center of the cylindrical duct, which indicates that bubbles near the symmetry axis are moving faster.

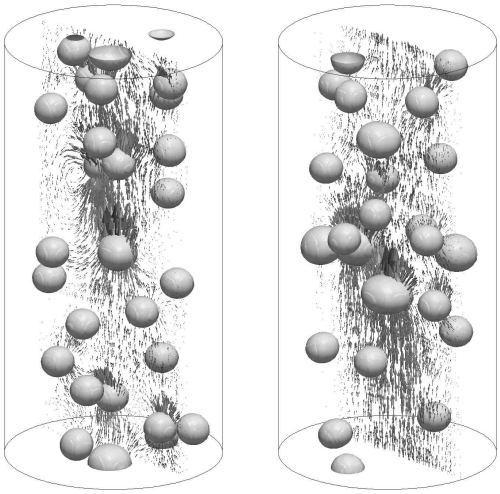

$t^* = 11.2$ $\qquad$ $t^* = 14.0$

Figure 3: Bubbly flow: $M = 6.0\times10^{-4}$, $Eo = 2.25$, $\rho_1/\rho_2 = 10$, $\mu_1/\mu_2 = 10$.

In the final paper the main features of the flow for different Eo and M numbers, will be discussed in detail.

REFERENCES

[1] Brackbill, J.U., Kothe, D.B., Zemach, C., 1992. A Continuum Method for Modeling Surface Tension, J. Comput. Phys. 100, 335-354.

[2] Olsson, E., Kreiss, G., 2005. A conservative level set method for two phase flow, J. Comput. Phys. 210, 225-246.

[3] Felten, F.N., Lund, T.S., 2006. Kinetic energy conservation issues associated with the collocated mesh scheme for incompressible flow, J. Comput. Phys. 215, 465-484

[4] Clift, R., Grace, J.R., Weber, M.E., Bubbles, Drops and Particles. Academin Press, New York, 1978.

[5] G. Brereton, D. Korotney, Coaxial and Oblique Coalescence of Two Rising Bubbles, in Dynamics of bubbles and Vortices Near a Free Surface, *ASME 119*, New York, 1991

DIRECT NUMERICAL SIMULATION OF A NACA0012 AIRFOIL WITH MASSIVE SEPARATION

I. Rodríguez[1], O. Lehmkuhl[1,2], R. Borrell[2], A.Oliva[1]
[1]Centre Tecnològic de Transferència de Calor (CTTC), Universitat Politècnica de Catalunya (UPC), Spain
[2] Termo Fluids S.L., Spain

INTRODUCTION

The flow around airfoils in full stall is a problem of great interest in aerodynamics and specifically for the design of turbo-machines (turbines, propellers, wind turbines, etc.). However, mechanisms of quasi-periodic oscillation observed near stall and stall behaviour, which affect airfoil efficiency, remain still not fully understood. Thus, the study of the separation mechanism and the correct prediction of boundary layer transition are both key aspects for improving engineering designs.

The advances in computational fluid dynamics together with the increasing capacity of parallel computers have made possible to tackle such complex turbulent problems by using high-performance numerical techniques such as direct numerical simulation (DNS) [1, 2]. DNS has a key role for improving the understanding of the turbulence phenomena and for the simulation of transitional flows in complex geometries In the present work DNS of the flow past a NACA0012 airfoil at $Re = 5 \times 10^4$ and angles of attack of 5°, 8°, 9.25° and 12° (the last one correspond to a full-stall situation) have been carried out. This work aims at investigating the mechanisms of separation and the prediction of the transition to turbulence in the separated shear-layer while at the same time to gain insight into coherent structures formed in the separated zone at lo-to-moderate Reynolds numbers.

DESCRIPTION OF NUMERICAL METHOD

The Navier-Stokes and continuity equations can be written as

$$\mathsf{M}u = 0 \tag{1}$$

$$\frac{\partial u}{\partial t} + \mathsf{C}(u)\,u + \nu \mathsf{D}u + \rho^{-1}\mathsf{G}p = 0 \tag{2}$$

where u and p are the velocity vector and pressure, respectively; ν is the kinematic viscosity and ρ the density. Convective and diffusive terms in the momentum equation for the velocity field are given by $\mathsf{C}(u) = (u\cdot\nabla)$ and $\mathsf{D} = -\nabla^2$ respectively. Gradient and divergence (of a vector) operators are given by $\mathsf{G} = \nabla$ and $\mathsf{M} = \nabla\cdot$, respectively.

The governing equations have been discretised on a collocated unstructured grid arrangement by means of second-order spectro-consistent schemes [3]. Such schemes are conservative, i.e. they preserve the kinetic energy equation. These conservation properties are held if, and only if the discrete convective operator is skew-symmetric ($\mathsf{C}_c(u_c) = -\mathsf{C_c}^*(u)$), the negative conjugate transpose of the discrete gradient operator is exactly equal to the divergence operator ($-(\Omega_c\mathsf{G}_c)^* = \mathsf{M}_c$) and the diffusive operator D_c, is symmetric and positive-definite (the sub-index c holds for the cell-centred discretisation). For the temporal discretization of the momentum equation, a two-step linear explicit scheme on a fractional-step method has been used [4], while for the pressure-gradient term an explicit first-order scheme has been used. The velocity-pressure coupling has been solved by means of a classical fractional step projection method,

$$u^p = u^{n+1} + \mathsf{G}\tilde{p} \tag{3}$$

where $\tilde{p} = p^{n+1}\Delta t^n/\rho$ is the pseudo-pressure, u^p the predicted velocity, $n+1$ is the instant where the temporal variables are calculated, and Δt^n is the current time step ($\Delta t^n = t^{n+1} - t^n$). Taking the divergence of (3) and applying the incompressibility condition yields a discrete Poisson equation for $\tilde{p}$: $\mathsf{L}\,\tilde{p} = \mathsf{M}\,u^p$. The discrete laplacian operator $\mathsf{L} \in \mathbb{R}^{m\times m}$ is, by construction, a symmetric positive definite matrix ($\mathsf{L} \equiv \mathsf{M}\Omega^{-1}\mathsf{M}^*$). Once the solution of p^{n+1} is obtained, $\tilde{p}$ results from equation 3. Finally the mass-conserving velocity at the faces ($\mathsf{M}_s u_s^{n+1} = 0$) is obtained from the correction,

$$u_s^{n+1} = u_s^p - \mathsf{G}_s\tilde{p} \tag{4}$$

where G_s represents the discrete gradient operator at the CV faces. This approximation allows to conserve mass at the faces. However, when the fractional step method on a collocated arrangement is used, there are two sources of errors in the kinetic energy conservation: i) due to interpolation schemes and, ii) due to inconsistency in the pressure field in order to ensure mass conservation. While the first one can be eliminated through the use of conservative schemes such as those used in the present work, the latter equals to [5, 6]:

$$\varepsilon_{\mathbf{ke}} = (\tilde{p_c})^*\mathsf{M}_c(\mathsf{G}_c - \mathsf{G}_s)\tilde{p_c} \tag{5}$$

This contribution of the pressure gradient term to the evolution of the kinetic energy can not be eliminated. Felten & Lund [6] have conducted a study to determine its scaling order. They have shown that the spatial term of the pressure error scales as $O(\Delta x^2)$ and the temporal term scales as $O(\Delta t)$, i.e. pressure errors are of the order of $O(\Delta x^2\,\Delta t)$. However, in their work they have proven that pressure errors do not have a significant impact on the results at grid resolutions and time-steps used in LES and in DNS. The methodology used have been proven to yield accurate results and have been previously used for solving the flow over bluff bodies with massive separation in [7] and [8].

RESULTS

All computed flows are around a NACA-0012 airfoil extended to include sharp trailing edge. All coordinates are referred to body axes unless remarked. The x axis is chord-wise, y is in the plane of the airfoil and z is spanwise direction. Solutions are obtained in a computational domain of dimensions $40C \times 40C \times 0.2C$ with the leading edge of the airfoil placed at $(0,0,0)$.The boundary conditions at the inflow consist of a uniform velocity profile (u,v,w)=($U_{ref}\cos AOA$, $U_{ref}\sin AOA$, 0). As for the outflow boundary, a pressure-based condition is imposed. No-slip conditions on the airfoil surface are prescribed. Periodic boundary conditions are used in the spanwise direction.

For carrying out the computations at the same grid has been used for the different AoA. Flow around an airfoil is mostly laminar with

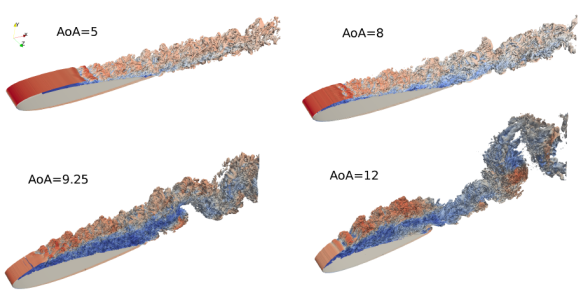

Figure 1: Instantaneous snapshots of vortical structures at different AoA

the exception of a zone close to the surface of the airfoil (suction side) and in the wake of it. When performing DNS, it must be ensured that the grid size is enough to solve the smallest flow scales well in the turbulent zones. Furthermore, within laminar zones, boundary layer must also be well-solved. Taking into account that the accuracy of the results is highly grid dependent, specially in the region of the separated shear-layer where transition to turbulence occurs, care must be taken when the computational grid is constructed. Another critical region is the near wake of the airfoil, where a poor grid resolution may cause notable upstream flow distortions. With these criteria, more control volumes have been clustered in these zones, but although the grid used is unstructured, it has been constructed as uniform as possible in the regions of interest. Thus, the results presented in the paper have been performed on a grid of about 46.6 million CVs (340526×128 planes) which covers the whole domain.

For obtaining the numerical results presented, the simulation starts from an initially homogeneous flow field which introduces some numerical disturbances as it is not the solution of the governing equations. These disturbances eventually causes the flow became three-dimensional and triggers transitions to turbulence. Then, simulation has been advanced in time until statistical stationary flow conditions have been achieved and the initial transient is completely washed out.

In order to gain insight into the coherent structures developed in the separated zone, instantaneous Q-iso surfaces have been depicted in figure 1 for the different AOA. The flow separates laminarly from the airfoil surface near the leading edge as can be inferred from the two-dimensional shear-layer developed. Vortex breakdown occurs at the end of the laminar shear-layer as a consequence of the instabilities developed by the action of a Kelvin-Helmholtz mechanism (see figure 1). These instabilities are high frequency fluctuations in the velocity which grow in magnitude as the distance from the leading edge increases and eventually causes shear layer to roll-up and undergo transition to turbulent flow, where these instabilities in the shear layer can be clearly seen, and how they increase their amplitude until finally transition to turbulence occurs). This mechanism of transition is similar to that observed in shear-layers developed in other bluff bodies such as the flow past a sphere [8].

Figure 2 shows the resulting energy spectra for the streamwise velocity fluctuations for AoA 12° of several probes located on the suction side and in the near wake. The energy spectra exhibit different ranges and fundamental frequencies, from transition to turbulent flow observed in the bottom curve (corresponding with probe P0) to the regular decay of slope close to $-5/3$ as the flow approaches the airfoil aft and flows into the wake (probe P5). This is indicative of the presence of an inertial subrange for more than a decade of frequencies. As for the significant frequencies, the spectrum for P0 shows a broadband peak at $f_{SL} = 9.74$ ($S_t = f\sin(AOA)C/U = 2.025$, here Strouhal is based on the airfoil projection on a cross-stream plane). This peak corresponds with

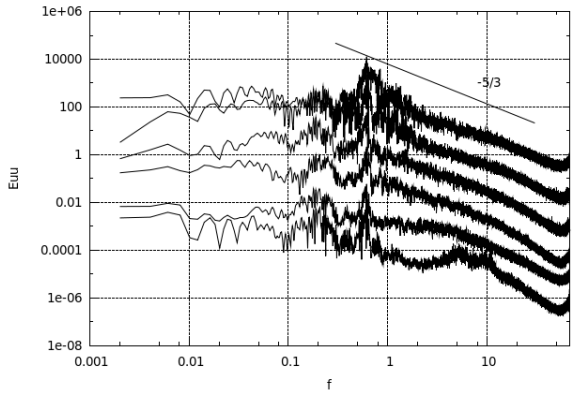

Figure 2: Energy spectra of the streamwise velocity fluctuations for $AOA = 12°$.

the frequency of the shear-layer instabilities and disappears as the flow moves downstream and the separated shear layer becomes turbulent. Note that it has only been captured by the probe located at ($x/C = 0.2$; $y/C = 0.125$) which is close to the separated shear layer.

In the final paper the main features of the flow for AoA of 5°, 8°, 9.25° and 12°, including power spectra of a set of selected monitoring probes at different positions in the suction side and in the near-wake of the airfoil will be discussed in detail.

REFERENCES

[1] A Baez, Lehmkuhl O., I. Rodriguez, and C.D. Perez-Segarra. Direct Numerical Simulation of the turbulent flow around a NACA 0012 airfoil at different angles of attack. In *Parallel CFD 2011*, 2011.

[2] O. Lehmkuhl, A. Baez, I. Rodríguez, and C. D. Perez-Segarra. Direct numerical simulation and Large-Eddy simulations of the turbulent flow around a NACA-0012 airfoil. In *7th International Conference on Computational Heat and Mass Transfer*, pages 1–8, 2011.

[3] R. W. C. P. Verstappen and A. E. P. Veldman. Symmetry-Preserving Discretization of Turbulent Flow. *Journal of Computational Physics*, 187:343–368, May 2003.

[4] F.X. Trias and O. Lehmkuhl. A self-adaptive strategy for the time integration of navier-stokes equations. *Numerical Heat Transfer. Part B*, 60(2):116–134, 2011.

[5] Y. Morinishi, T.S. Lund, O.V. Vasilyev, and P. Moin. Fully conservative higher order finite difference schemes for incompressible flow. *Journal of Computational Physics*, 143(1):90–124, 1998.

[6] F.N. Felten and T.S. Lund. Kinetic energy conservation issues associated with the collocated mesh scheme for incompressible flow. *Journal of Computational Physics*, 215(2):465–484, 2006.

[7] O. Lehmkuhl, R. Borrell, J. Chivas, and C.D. Perez-Segarra. Direct numerical simulations and symmetry-preserving regularization simulations of the flow over a circular cylinder at Reynolds number 3900. In *Turbulence, Heat and Mass Transfer*, 2009.

[8] I. Rodríguez, R. Borrell, O. Lehmkuhl, C.D. Pérez-Segarra, and A. Oliva. Direct Numerical Simulation of the Flow Over a Sphere at Re = 3700. *Journal of Fluids Mechanics*, 679:263–287, 2011.

NEW DIFFERENTIAL OPERATORS AND DISCRETIZATION METHODS FOR EDDY-VISCOSITY MODELS FOR LES

F.Xavier Trias[1], Andrey Gorobets[1,2] & Assensi Oliva[1]
[1]*Heat and Mass Transfer Technological Center, Technical University of Catalonia*
ETSEIAT, C/Colom 11, 08222 Terrassa, Spain
[2] *Keldysh Institute of Applied Mathematics, 4A, Miusskaya Sq., Moscow 125047, Russia*

Abstract The incompressible Navier-Stokes equations constitute an excellent mathematical modelization of turbulence. Unfortunately, attempts at performing direct simulations are limited to relatively low-Reynolds numbers. Therefore, dynamically less complex mathematical formulations are necessary for coarse-grain simulations. Eddy-viscosity models for Large-Eddy Simulation (LES) is an example thereof: they rely on differential operators that should be able to capture well different flow configurations (laminar and 2D flows, near-wall behavior, transitional regime...). In the present work, several differential operators are derived from the criterion that vortex-stretching mechanism must stop at the smallest grid scale. Moreover, since the discretization errors may play an important role a novel approach to discretize the viscous term with spatially varying eddy-viscosity is used. It is based on basic operators; therefore, the implementation is straightforward even for staggered formulations.

INTRODUCTION

We consider the simulation of the incompressible Navier-Stokes (NS) equations. In primitive variables they read

$$\partial_t \boldsymbol{u} + \mathcal{C}(\boldsymbol{u},\boldsymbol{u}) = \mathcal{D}\boldsymbol{u} - \nabla p, \qquad \nabla\cdot\boldsymbol{u} = 0, \tag{1}$$

where $\boldsymbol{u}$ denotes the velocity field, p represents the pressure, the non-linear convective term is given by $\mathcal{C}(\boldsymbol{u},\boldsymbol{v}) = (\boldsymbol{u}\cdot\nabla)\,\boldsymbol{v}$, and the diffusive term reads $\mathcal{D}\boldsymbol{u} = \nu\Delta\boldsymbol{u}$, where ν is the kinematic viscosity. Direct simulations at high Reynolds numbers are not feasible because the convective term produces many scales of motion. Hence, in the foreseeable future numerical simulations of turbulent flows will have to resort to models of the small scales. The most popular example thereof is the Large-Eddy Simulation (LES). Shortly, LES equations result from filtering the NS equations in space

$$\partial_t \overline{\boldsymbol{u}} + \mathcal{C}(\overline{\boldsymbol{u}},\overline{\boldsymbol{u}}) = \mathcal{D}\overline{\boldsymbol{u}} - \nabla\overline{p} - \nabla\cdot\tau(\overline{\boldsymbol{u}})\ ; \qquad \nabla\cdot\overline{\boldsymbol{u}} = 0, \tag{2}$$

where $\overline{\boldsymbol{u}}$ is the filtered velocity and $\tau(\overline{\boldsymbol{u}})$ is the subgrid stress tensor and approximates the effect of the under-resolved scales, *i.e.* $\tau(\overline{\boldsymbol{u}}) \approx \overline{\boldsymbol{u}\otimes\boldsymbol{u}} - \overline{\boldsymbol{u}}\otimes\overline{\boldsymbol{u}}$. Then, the closure problem consists on replacing (approximating) the tensor $\overline{\boldsymbol{u}\otimes\boldsymbol{u}}$ with a tensor depending only on $\overline{\boldsymbol{u}}$ (and not $\boldsymbol{u}$). Because of its inherent simplicity and robustness, the eddy-viscosity assumption is by far the most used closure model

$$\tau(\overline{\boldsymbol{u}}) \approx -2\nu_e S(\overline{\boldsymbol{u}}), \tag{3}$$

where ν_e denotes the eddy-viscosity and $\tau(\overline{\boldsymbol{u}})$ is considered traceless without the loss of generality.

RESTRAINING THE PRODUCTION OF SMALL SCALES

The essence of turbulence are the smallest scales of motion. They result from a subtle balance between convective transport and diffusive dissipation. Numerically, if the grid is not fine enough, this balance needs to be restored by a turbulence model. Hence, the success of a turbulence model depends on the ability to capture well this (im)balance. Let us consider an arbitrary part of the domain flow, Ω, with periodic boundary conditions. The inner product is defined in the usual way: $(a,b) = \int_\Omega a\cdot b d\Omega$. Then, taking the L^2 inner product of (1) with $-\Delta\boldsymbol{u}$ leads to the enstrophy equation

$$1/2\|\boldsymbol{\omega}\|_t^2 = (\boldsymbol{\omega},\mathcal{C}(\boldsymbol{\omega},\boldsymbol{u})) - \nu(\nabla\boldsymbol{\omega},\nabla\boldsymbol{\omega}), \tag{4}$$

where $\|\boldsymbol{\omega}\|^2 = (\boldsymbol{\omega},\boldsymbol{\omega})$ and the convective term contribution $(\mathcal{C}(\boldsymbol{u},\boldsymbol{\omega}),\boldsymbol{\omega}) = 0$ vanishes because of the skew-symmetry of $\mathcal{C}$. Following [3], the vortex-stretching term can be expressed in terms of the invariant $R = -1/3tr(S^3) = -det(S)$

$$(\boldsymbol{\omega},\mathcal{C}(\boldsymbol{\omega},\boldsymbol{u})) = -\frac{4}{3}\int_\Omega tr(S^3)d\Omega = 4\int_\Omega R d\Omega = 4\widetilde{R}, \tag{5}$$

whereas the diffusive terms may be bounded in terms of the invariant $Q = -1/2tr(S^2)$

$$(\nabla\boldsymbol{\omega},\nabla\boldsymbol{\omega}) = -(\boldsymbol{\omega},\Delta\boldsymbol{\omega}) \leq -\lambda_\Delta(\boldsymbol{\omega},\boldsymbol{\omega}) = 4\lambda_\Delta\int_\Omega Q d\Omega = 4\lambda_\Delta\widetilde{Q}, \tag{6}$$

where $\lambda_\Delta < 0$ is the largest (smallest in absolute value) non-zero eigenvalue of the Laplacian operator Δ on Ω and $\widetilde{(\cdot)}$ denotes the integral over Ω. However, it relies on the accurate estimation of λ_Δ on Ω. The latter may be cumbersome,

especially on unstructured grids. Alternatively, it may be (numerically) computed directly from $(\nabla\boldsymbol{\omega},\nabla\boldsymbol{\omega})$ or, even easier, by simply noticing that $(\nabla\boldsymbol{\omega},\nabla\boldsymbol{\omega}) = 4\int_\Omega Q(\boldsymbol{\omega})d\Omega = 4\widetilde{Q(\boldsymbol{\omega})}$. However, from a numerical point-of-view, these integrations are not straightforward. Instead, recalling that $\nabla\times\nabla\times\boldsymbol{u} = \nabla(\nabla\cdot\boldsymbol{u}) - \Delta\boldsymbol{u}$ and $\nabla\cdot\boldsymbol{u} = 0$, a more appropriate expression can be obtained as follows

$$(\nabla\boldsymbol{\omega},\nabla\boldsymbol{\omega}) = -(\boldsymbol{\omega},\Delta\boldsymbol{\omega}) = (\boldsymbol{\omega},\nabla\times\nabla\times\boldsymbol{\omega}) = (\nabla\times\boldsymbol{\omega},\nabla\times\boldsymbol{\omega}) = (\Delta\boldsymbol{u},\Delta\boldsymbol{u}) = \|\Delta\boldsymbol{u}\|^2. \tag{7}$$

Then, to prevent a local intensification of vorticity, *i.e.* $\|\boldsymbol{\omega}\|_t \leq 0$, the inequality $H_\Omega \leq \nu(\Delta\boldsymbol{u},\Delta\boldsymbol{u})/(\boldsymbol{\omega},S\boldsymbol{\omega})$ must be satisfied, where H_Ω denotes the overall damping introduced by the model in the (small) part of the domain Ω. Additionally, the dynamics of the large scales should not be significantly affected by the (small) scales contained within the domain Ω, *i.e.* $(\boldsymbol{\omega},S\boldsymbol{\omega}) < 0$. Then, from Eq.(5) and noticing that $0 < H_\Omega \leq 1$, a proper definition of the overall damping factor follows $H_\Omega = \min\left\{\nu\|\Delta\boldsymbol{u}\|^2/|\widetilde{R}|, 1\right\}$. An eddy-viscosity model, $\tau(\overline{\boldsymbol{u}}) = -2\nu_e S(\overline{\boldsymbol{u}})$, adds the dissipation term $(\nabla\overline{\boldsymbol{\omega}},\nu_e\nabla\overline{\boldsymbol{\omega}})$ to the enstrophy equation. In this case, the eddy-viscosity, ν_e, results

$$\nu_e = \max\left\{(4|\widetilde{R}| - \nu\|\Delta\overline{\boldsymbol{u}}\|^2)/\|\Delta\overline{\boldsymbol{u}}\|^2, 0\right\}. \tag{8}$$

This analysis can be extended further for other differential operators. For instance, $\tau'(\overline{\boldsymbol{u}}) = 2\nu_e' S(\Delta\overline{\boldsymbol{u}})$ and $\tau''(\overline{\boldsymbol{u}}) = -2\nu_e'' S(\Delta^2\overline{\boldsymbol{u}})$, where $\Delta^2 \equiv \Delta\Delta$ is the bi-Laplacian, lead to the following hyperviscosity terms in the enstrophy equation $-(\nabla\overline{\boldsymbol{\omega}},\nu_e'\nabla\Delta\overline{\boldsymbol{\omega}})$ and $(\nabla\overline{\boldsymbol{\omega}},\nu_e''\nabla\Delta^2\overline{\boldsymbol{\omega}})$. Then, following similar reasonings, ν_e' and ν_e'' follow

$$\nu_e' = \max\left\{-(4|\widetilde{R}| - \nu\|\Delta\overline{\boldsymbol{u}}\|^2)/(\Delta\overline{\boldsymbol{u}},\Delta^2\overline{\boldsymbol{u}}), 0\right\} \quad \text{and} \quad \nu_e'' = \max\left\{(4|\widetilde{R}| - \nu\|\Delta\overline{\boldsymbol{u}}\|^2)/\|\Delta^2\overline{\boldsymbol{u}}\|^2, 0\right\}. \tag{9}$$

DISCRETIZING THE VISCOUS TERM WITH SPATIALLY VARYING EDDY-VISCOSITY

The NS equations (1) with constant physical properties are discretized on a staggered grid using a fourth-order symmetry-preserving discretization [4]. Here we propose to apply the same ideas to discretize the eddy-viscosity model (3) for LES (2). To obtain the Eq.(1) (with ν replaced by $\nu+\nu_e$) from Eqs.(2)-(3) with constant ν_e notice that $2\nabla\cdot S(\boldsymbol{u}) = \nabla\cdot\nabla\boldsymbol{u} + \nabla\cdot(\nabla\boldsymbol{u})^T$ and recall the vector calculus identity $\nabla\cdot(\nabla\boldsymbol{u})^T = \nabla(\nabla\cdot\boldsymbol{u})$ to cancel out the second term. However, for non-constant ν_e, the discretization of $\nabla\cdot(\nu_e(\nabla\boldsymbol{u})^T)$ needs to be addressed. This can be quite cumbersome especially for staggered formulations. The standard approach consist on discretizing the term $\nabla\cdot(\nu_e(\nabla\boldsymbol{u})^T)$ directly. However, this implies many *ad hoc* interpolations that tends to smear the eddy-viscosity, ν_e. This may (negatively?) influence the performance of eddy-viscosity especially near the walls. Instead, an alternative form was proposed in [2]. Shortly, with the help of vector calculus it can be shown that $\nabla\cdot(\nu_e(\nabla\boldsymbol{u})^T) = \nabla(\nabla\cdot(\nu_e\boldsymbol{u})) - \nabla\cdot(\boldsymbol{u}\otimes\nabla\nu_e)$. Then, recalling that the flow is incompressible, the second term in the right-hand-side can be written as $\nabla\cdot(\boldsymbol{u}\otimes\nabla\nu_e) = (\boldsymbol{u}\cdot\nabla)\nabla\nu_e = \mathcal{C}(\boldsymbol{u},\nabla\nu_e)$, *i.e.*

$$\nabla\cdot(\nu_e(\nabla\boldsymbol{u})^T) = \nabla(\nabla\cdot(\nu_e\boldsymbol{u})) - \mathcal{C}(\boldsymbol{u},\nabla\nu_e). \tag{10}$$

In this way, consistent approximations of Eqs.(2)-(3) can be constructed without introducing new interpolation operators.

CONCLUDING REMARKS AND FUTURE RESEARCH

In the context of LES, three eddy-viscosity-type models have been obtained. Namely, (i) $\tau(\overline{\boldsymbol{u}}) = -2\nu_e S(\overline{\boldsymbol{u}})$, (ii) $\tau'(\overline{\boldsymbol{u}}) = 2\nu_e' S(\Delta\overline{\boldsymbol{u}})$ and (iii) $\tau''(\overline{\boldsymbol{u}}) = -2\nu_e'' S(\Delta^2\overline{\boldsymbol{u}})$, where ν_e, ν_e' and ν_e'' are given by Eqs.(8) and (9), respectively. Notice that, apart from R, these models can be straightforwardly implemented by re-using the discrete diffusive operator. They can be related with already existing approaches. Firstly, the model (i) is almost the same than the recently proposed QR-model [3]. Essentially, they only differ on the calculation of the diffusive contribution to the enstrophy equation: instead of making use of the equality (7) it is bounded by means of the inequality (6), therefore, the eddy-viscosity is given by $\nu_e \propto \lambda_\Delta^{-1}|\widetilde{R}|/\widetilde{Q}$ instead of Eq.(8). Regarding the models (ii) and (iii) they can be respectively related to the well-known small-large and small-small variational multiscale methods [1] by noticing that $\boldsymbol{u}' = -(\epsilon^2/24)\Delta\boldsymbol{u} + \mathcal{O}(\epsilon^4)$. All these models switch off ($R\to 0$) for laminar (no vortex-stretching), 2D flows ($\lambda_2 = 0 \to R = 0$) and near the wall ($R \propto y^1$). To test the performance of these new turbulence models in conjunction with the new discretization approach is part of our research plans. In particular, we plan to test them for a turbulent channel flow and square duct at $Re_\tau = 1200$.

References

[1] T. J. R. Hughes, L. Mazzei, A. A. Oberai, and A. A. Wray. The multiscale formulation of large eddy simulation: Decay of homogeneous isotropic turbulence. *Physics of Fluids*, **13**(2):505–512, 2001.

[2] F. X. Trias, A. Gorobets, and A. Oliva. A simple approach to discretize the viscous term with spatially varying (eddy-)viscosity. *Journal of Computational Physics*, **253**:405–417, 2013.

[3] R. Verstappen. When does eddy viscosity damp subfilter scales sufficiently? *Journal of Scientific Computing*, **49**(1):94–110, 2011.

[4] R. W. C. P. Verstappen and A. E. P. Veldman. Symmetry-Preserving Discretization of Turbulent Flow. *Journal of Computational Physics*, **187**:343–368, 2003.

ON THE LARGE-EDDY SIMULATIONS OF THE FLOW PAST A CYLINDER AT CRITICAL REYNOLDS NUMBERS

O. Lehmkuhl[1,2], I. Rodríguez[1], J. Chiva[1] and R. Borrell[1,2]
[1] Heat and Mass Transfer Technological Center, UPC, Spain
[2] Termo Fluids S.L, Spain

INTRODUCTION

The flow past a circular cylinder is associated with various instabilities which involve the wake, separated shear layer and boundary layer.It is well known that when Reynolds numbers is about 2×10^5 the boundary layer undergoes a transition from laminar to turbulent regime. The range of critical Reynolds numbers up to $\sim 5\times10^5$ is characterised by a rapid decrease of the drag coefficient with the Reynolds numbers. Other features characterise this regime, such a the presence an asymmetric laminar separation bubble as reported experimentally by Bearman [1]. This work aims at shed some light into the complex physics present at these critical Reynolds numbers by means of large-eddy simulations of the flow.

DESCRIPTION OF NUMERICAL METHOD

In the quest for a correct modelling of Navier-Stokes equations, they can be filtered spatially as in Large-Eddy Simulations (LES),

$$\mathcal{M}\overline{\boldsymbol{u}} = \boldsymbol{0} \quad (1)$$

$$\Omega\frac{\partial\overline{\boldsymbol{u}}}{\partial t} + \mathsf{C}\left(\overline{\boldsymbol{u}}\right)\overline{\boldsymbol{u}} + \nu\mathsf{D}\overline{\boldsymbol{u}} + \rho^{-1}\Omega\mathsf{G}\overline{\boldsymbol{p}} = \mathsf{C}\left(\overline{\boldsymbol{u}}\right)\overline{\boldsymbol{u}} - \overline{\mathsf{C}\left(\boldsymbol{u}\right)\boldsymbol{u}} \approx -\mathcal{M}\mathcal{T} \quad (2)$$

where $\overline{\boldsymbol{u}}\in\mathbb{R}^{3m}$ and $\overline{\boldsymbol{p}}\in\mathbb{R}^{m}$ are the filtered velocity vector and pressure, respectively (here m applies for the total number of control volumes (CV) of the discretised domain), ν is the kinematic viscosity and ρ the density. $\Omega\in\mathbb{R}^{3m}$ is a matrix with the cell control volumes. Convective and diffusive operators in the momentum equation for the velocity field are given by $\mathsf{C}\left(\overline{\boldsymbol{u}}\right)=\left(\overline{\boldsymbol{u}}\cdot\nabla\right)\in\mathbb{R}^{3m\times3m}$, $\mathsf{D}=-\nabla^2\in\mathbb{R}^{3m\times3m}$ respectively. Gradient and divergence (of a vector) operators are given by $\mathsf{G}=\nabla\in\mathbb{R}^{3m\times m}$ and $\mathcal{M}=\boldsymbol{\nabla}\cdot\in\mathbb{R}^{m\times3m}$ respectively. The last term indicates some modelisation of the filtered non-linear convective term. $\mathcal{T}$ is the SGS stress tensor, which is defined as,

$$\mathcal{T} = -2\nu_{sgs}\mathcal{S}_{ij} + (\mathcal{T}:\boldsymbol{I})\boldsymbol{I}/3 \quad (3)$$

where $\mathcal{S}_{ij}=\frac{1}{2}[\mathsf{G}(\overline{\boldsymbol{u}})+\mathsf{G}^*(\overline{\boldsymbol{u}})]$, and G^* is the transpose of the gradient operator. To close the formulation, a suitable expression for the subgrid-scale (SGS) viscosity must be introduced. LES studies have been performed using the wall-adapting local-eddy viscosity model within a variational multi-scale framework (VMS-WALE) [2, 3]. The variational multi-scale (VMS) approach was originally formulated for the Smagorinsky model by Hughes [3] is used here with the *small-small* strategy is used in conjunction with the wall-adapting eddy viscosity (WALE) model [2]. In VMS three classes of scales are considered: large, small and unresolved scales. If a second filter with filter length $\hat{\ell}$ is introduced (usually called test filter), a splitting of the scales can be performed, $f^{'}=\overline{f}-\hat{f}$. For the large-scale parts of the resolved $\overline{\boldsymbol{u}}$ a general governing equation can be derived,

$$\frac{\partial\overline{\boldsymbol{u}}}{\partial t} + \mathsf{C}\left(\overline{\boldsymbol{u}}\right)\overline{\boldsymbol{u}} + \nu\mathsf{D}\overline{\boldsymbol{u}} + \rho^{-1}\Omega\mathsf{G}\overline{\boldsymbol{p}} = -\frac{\partial\widehat{\mathcal{T}}}{\partial x_j} - \frac{\partial\mathcal{T}^{'}}{\partial x_j} \quad (4)$$

Neglecting the effect of unresolved scales in the large-scale equation ($\widehat{\mathcal{T}}\approx0$), it is only necessary to model the $\mathcal{T}^{'}$.

$$\begin{aligned}
\mathcal{T}^{'} &= -2\nu_{sgs}\mathcal{S}_{\mathrm{ij}}{}^{'} + \frac{1}{3}\mathcal{T}^{'}\delta_{ij} \quad (5)\\
\nu_{sgs} &= (C_w^{vms}\ell)^2\frac{(\mathcal{V}_{\mathrm{ij}}{}^{'}:\mathcal{V}_{\mathrm{ij}}{}^{'})^{\frac{3}{2}}}{(\mathcal{S}_{\mathrm{ij}}{}^{'}:\mathcal{S}_{\mathrm{ij}}{}^{'})^{\frac{5}{2}}+(\mathcal{V}_{\mathrm{ij}}{}^{'}:\mathcal{V}_{\mathrm{ij}}{}^{'})^{\frac{5}{4}}}\\
\mathcal{S}_{\mathrm{ij}}{}^{'} &= \frac{1}{2}[\mathsf{G}(\overline{\boldsymbol{u}'})+\mathsf{G}^*(\overline{\boldsymbol{u}'})]\\
\mathcal{V}_{\mathrm{ij}}{}^{'} &= \frac{1}{2}[\mathsf{G}(\overline{\boldsymbol{u}'})^2+\mathsf{G}^*(\overline{\boldsymbol{u}'})^2] - \frac{1}{3}(\mathsf{G}(\overline{\boldsymbol{u}'})^2\boldsymbol{I})
\end{aligned}$$

where C_w^{vms} is the equivalent of the WALE coefficient for the *small-small* VMS approach and in the finite volume context its value lies in the range between 0.3 and 0.5. In our studies a value of 0.325 is used.

The governing equations have been discretised on a collocated unstructured grid arrangement by means of second-order spectro-consistent schemes. Such schemes are conservative, i.e. they preserve the symmetry properties of the continuous differential operators and ensure both, stability and conservation of the kinetic-energy balance even at high Reynolds numbers and with coarse grids. For the temporal discretisation of the momentum equation (2) a two-step linear explicit scheme on a fractional-step method has been used for the convective and diffusive terms [4], while for the pressure gradient term an implicit first-order scheme has been implemented. This methodology has been previously used with accurate results for solving the flow over bluff bodies with massive separation [5, 6].

RESULTS

We consider here the flow past a circular cylinder at critical Reynolds numbers of $Re_D = 1.44\times10^5$, 2.6×10^5, 3.8×10^5

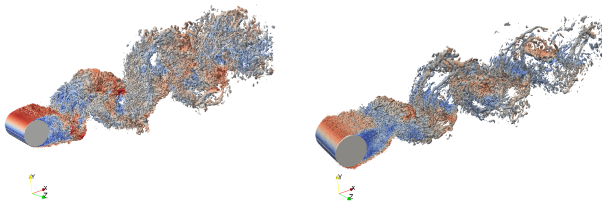

Figure 1: Vortical structures at different Reynolds numbers (left) $Re = 1.4 \times 10^5$; (right) $Re = 5.3 \times 10^5$.

and 5.3×10^5. The cases have been solved in a computational domain of dimensions [-16D,16D];[-10D,10D];[0,0.5πD] in the stream-, cross- and span-wise directions, respectively, with a circular cylinder of diameter D at (0,0,0). The boundary conditions at the inflow consist of a uniform velocity (u,v,w)=(1,0,0), slip conditions in the top and bottom boundaries of the domain, while at the outlet a pressure-based condition is used. At the cylinder surface, no-slip conditions are prescribed. As for the span-wise direction, periodic boundary conditions are imposed. As mentioned before, the governing equations are discretised on an unstructured mesh generated by the constant-step extrusion of a two-dimensional unstructured grid. Different grids have been used, depending on the Reynolds numbers up to 387492×128 ($\sim$ 50MCV).

Figure 1 shows the isocontours of second invariant of the velocity gradient tensor coloured by the velocity magnitude at Reynolds numbers $Re = 1.4 \times 10^5$ and $Re = 5.3 \times 10^5$. While the lower Reynolds numbers exhibits a flow topology similar to that observed in the sub-critical regime, i.e. laminar flow separation and transition to turbulence in the separated shear layers, the flow at $Re = 5.3 \times 10^5$ shows a narrow wake with separation point moving towards the rear end of the cylinder.

The variation of the drag coefficient with the Reynolds number is plotted in figure 2 together with reference data from the literature. At these Reynolds numbers, the measured data of the drag coefficient present a large scattering because of the difficulties associated with the measurements, the flow is very sensitive to the different turbulence intensities, end conditions, surface roughness, etc. Even though this scattering in the reference data, results obtained with the present simulations shows a fair agreement. One interesting feature observed in the present computations is the presence of an asymmetric laminar bubble in the cylinder surface at $Re = 2.6 \times 10^5$. This asymmetric bubble which causes large fluctuations in the cylinder forces with average lift $C_l > 0$, was observed by Bearman [1] in his experiments, but its difficult to detect as it occurs in a narrow range of Reynolds numbers. At the larger Reynolds, $Re = 3.8 \times 10^5$ and $Re = 5.3 \times 10^5$, two bubbles are observed at each side of the cylinder surface, recovering the symmetry of the flow. In the final version of the manuscript, results of the different flow configurations observed at the different Reynolds numbers will be given, together with measurements of the local forces and characteristics frequencies of the flow.

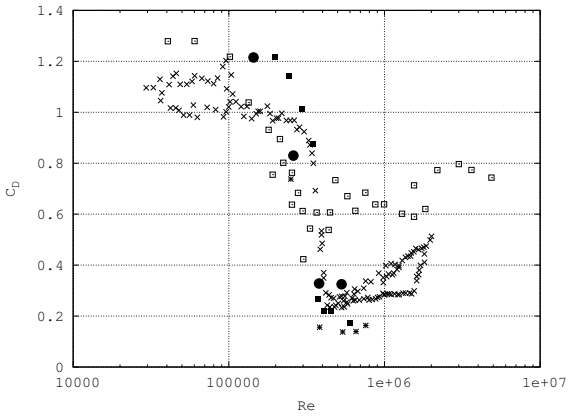

Figure 2: Variation of the drag coefficient with the Reynolds number. Comparison with the literature. (Solid dots) Present results, (squares) Achenbach [7], (solid squares) Bursnall and Loftin [8], (stars) Spitzer [9], (crosses) Delany and Sorensen [10]

REFERENCES

[1] PW Bearman. On vortex shedding from a circular cylinder in the critical Reynolds number regime. *J. Fluid Mech*, 37:577–585, 1969.

[2] F. Nicoud and F. Ducros. Subgrid-scale stress modelling based on the square of the velocity gradient tensor. *Flow, Turbulence and Combustion*, 62:183–200, 1999.

[3] T.J.R. Hughes, L. Mazzei, and K.E. Jansen. Large eddy simulation and the variational multiscale method. *Computing and Visualization in Science*, 3:47–59, 2000.

[4] F.X. Trias and O. Lehmkuhl. A self-adaptive strategy for the time integration of navier-stokes equations. *Numerical Heat Transfer. Part B*, 60(2):116–134, 2011.

[5] I. Rodríguez, R. Borrell, O. Lehmkuhl, C.D. Pérez-Segarra, and A. Oliva. Direct Numerical Simulation of the Flow Over a Sphere at Re = 3700. *Journal of Fluids Mechanics*, 679:263–287, 2011.

[6] I. Rodríguez, O. Lehmkuhl, R. Borrell, and A. Oliva. Flow dynamics in the wake of a sphere at sub-critical Reynolds numbers. *Computers & Fluids 10.1016/j.compfluid.2012.03.009*, 2012.

[7] E. Achenbach. Distribution of local pressure and slin friction around a circular cylinder in cross-flow up to Re=5e6. *J. Fluid Mech*, 34:625–639, 1968.

[8] WJ Bursnall and L.K. Jr Loftin. Experimental investigation of the pressure distribution about a yawed circular cylinder in the critical Reynolds number range. Technical Report NACA TN2463, NACA, 1951.

[9] R.E. Spitzer. *Measurements of unsteady pressures and wake fluctuations for flow over a cylinder at supercritical Reynolds number*. PhD thesis, California Institute of Technology, 1964.

[10] NK Delany and NE Sorensen. Low-speed drag of cylinders of various shapes. Technical Report NACA TN3038, NACA, 1953.

Turbulent jets in iron casting

R. Castilla[a], G. Raush[a], E. Dalmau[a], D. del Campo[b] and E. Codina[a]

[a] LABSON - Department of Fluid Mechanics. Politechnical University of Catalonia.
[b] ETSEIAT – Department of Aeronautics. Politechnical University of Catalonia.

ABSTRACT

Into the frame of the EU Project Flexicast, the Research Centre LABSON, in the UPC, is performing several numerical simulations of complex flows related to the iron casting process. In this workshop we present two of the simulations.

Firstly, the simulation of the pouring process in a tilting tank is simulated. The simulation has been performed with a moving reference frame, where the gravity vector is being rotated. Also the Coriolis and the centrifugal forces have been considered.

Secondly, the filling of a mould with a vertical jet is simulated. The aim is to enhance the mixing process of some additives in the fluid jet. RAS and LES turbulent models are being tested, and the results will be validated with experimental tests.

These simulations are being performed with the Open Source package OpenFoam, with the VOF model for the two phase flows.

TRANSIENT AND DYNAMIC NUMERICAL SIMULATION OF THE FLUID FLOW THROUGH VALVES BASED ON LARGE EDDY SIMULATION MODELS

J. Rigola[1], O. Estruch[1], O. Lehmkuhl[1,2], A.Oliva[1], C.D. Pérez-Segarra[1]
[1]Centre Tecnològic de Transferència de Calor (CTTC), Universitat Politècnica de Catalunya (UPC), Spain
[2] Termo Fluids S.L., Spain

INTRODUCTION

In the majority of hermetic reciprocating compressors valves are a basic component of both the suction and discharge ports and, particularly, reed type valves are widely used for domestic or commercial reciprocating compressors. The understanding of the behaviour of the fluid flow through the valve plate and moreover the dynamic action of the valve reed is essential to improve the compressor design and to contribute in the efficiency optimization. Few works in the literature consider a computational model to simulate the dynamics of reed type valves of reciprocating compressors. Thus, the present paper attempts the dynamic simulation of the fluid flow through the suction valve reed including an inlet port valve condition according to valve movement due to piston displacement and modelling the valve reed by means of a specific law based on modal analysis of valve reed theory [1].

In the following study, the transient simulation of the fluid and valve interaction is performed by means of the newly in-house implemented CFD&HT and moving mesh coupled code TermoFluids [2, 3]. This work extends previous studies, in which numerical experiments were carried out considering static geometry and constant boundary conditions [4]. As a preliminary approach, a simplified geometry of an axial hole plus a rectangular valve reed is considered.

DESCRIPTION OF THE NUMERICAL METHOD

For the present work the governing equations correspond to the incompressible Navier-Stokes and continuity equations coupled with dynamic mesh, which have been discretized on a collocated unstructured grid arrangement by means of second-order spectro-consistent schemes. Such schemes are conservative, *i.e.* they preserve the kinetic energy equation. For the temporal discretization of the momentum equation a fully explicit second-order self-adaptive scheme [5] has been used for the convective and difussive terms, while for the pressure gradient term an implicit first-order scheme has been used. The velocity-pressure coupling has been solved by means of a classical fractional step projection method. Large eddy simulation has been performed to model the turbulent flow through the wall-adapting local-eddy viscosity model (WALE) [6], available in TermoFluids.

A moving grid technique has been used in order to dynamically adapt the computational mesh to the valve deformation. Such technique is based on Radial Basis Function (RBF) interpolation (see [3]). The CFD and dynamic mesh coupling has been carried out by means of the so-called Space Conservation Law.

As a first approach we consider a simplified geometry of an axial hole plus a radial diffuser, which is considered like a flexible reed valve. Then, referring to [1], the dynamic action of the valve is based on a specific law according modal analysis of valve reed theory. This methodology assumes that the valve motion results from the superposition of the valve vibration modes. Thus, the deflection function is

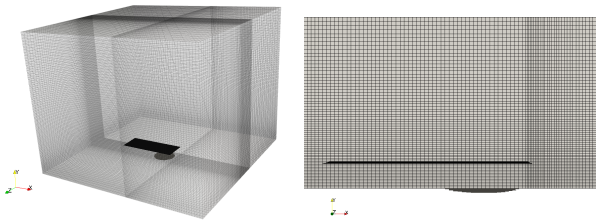

Figure 1: Computational mesh and domain. General view (left); zoom view (right).

expressed as a combination of the natural modes of the reed valve,

$$w(x,y,t) = \sum_{m=1}^{\infty} q_m(t)\phi_m(x,y) \tag{1}$$

The equation of motion leads to the following generalized equation, considering a valve reed of arbitrary geometry with k port holes,

$$\ddot{q}_m^{(t)} + 2\xi\omega_m\dot{q}_m^{(t)} + \omega_m^2 q_m^{(t)} = \frac{\Delta p(t)\sum_{m=1}^{k}\phi_m(x_i,y_i)A_F(w(x_i,y_i))\Delta A_i}{A\rho h\sum_{j=1}^{l}\phi_m^2(x_j,y_j)\Delta A_j} \tag{2}$$

where ϕ_m denote the shape of the natural modes, ω_m the natural frequencies, Δp the pressure differential across the valve, ξ the damping coefficient, A_F the effective force area, δA_i the area of the port hole at location (x_i, y_i), A the total port area, ΔA_j the area of the geometric discretizetion elements of the valve reed. In this study only the first main natural mode is considered. The parameters of the valve dynamics are $\xi = 0.056$, $\omega_0 = 1132.15 rad/s$, $\phi(x_1,y_1) = 5.39\cdot 10^3$, $\rho = 7870 kg/m^3$, $h = 2\cdot 10^{-4} m$ and $\sum_{j=1}^{l}\phi^2(x_j,y_j)\Delta A_j = 4.96\cdot 10^3 m^2$. The effective force area is extracted from the analytical method presented in (25).

COMPUTATIONAL DOMAIN, MESH AND BOUNDARY CONDITIONS

Figure 1 illustrates the computational mesh and domain containing the rectangular reed type valve. In the figure the inlet port hole of the suction valve is pointed out. The dimensions of the global domain are $L = 0.08m$ and $H = 0.06m$. The hole is centred at the bottom base, and its diameter is $d = 9.75\cdot 10^{-3} m$. The valve dimensions are: length $l = 0.026m$, width $w = 0.01m$ and thickness $h = 2\cdot 10^{-4} m$. The height of the axial hole is $e = 3.6\cdot 10^{-3} m$. In the initial configuration the valve is completely closed, i.e. is contained in the plane $y = 3.6\cdot 10^{-3}$, and it is translated $t = 6\cdot 10^{-3} m$ in the x direction. The computational mesh is structured and has over 2.5 million CVs.

For the bottom inlet orifice a piston based inlet condition is assumed (see Figure 2), which is defined with a frequency of $50Hz$. A pressure based boundary condition applies for the outlet fluid exit (lateral and top walls). Non-slip boundary conditions are considered on solid walls

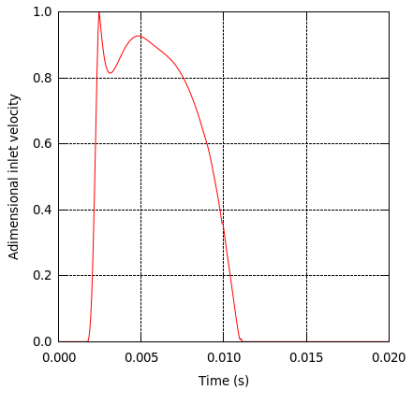

Figure 2: Piston based inlet boundary condition.

(bottom part amb valve reed). An immersed body procedure is used to simulate solid parts inside the domain and, hence, to reproduce the inlet and bottom boundaries. Therefore, the RBF method allows the simulation from null valve deformation.

RESULTS

The results presented in this section pretend to be a preliminary illustrative study of the transient and dynamic simulation of the fluid flow through a suction valve reed subjected to a piston based inlet condition and considering a modal model for the valve dynamics. In Figure 3 the hole centre deflection as function of time during a complete suction valve opening cycle is depicted. The period of time in which the valve reed remains opened corresponds with the period of existing inlet flux (see Figure 2), although the valve reed appears to become completely closed with a little delay. During the opened stage, three peaks of oscillation can be appreciated, each of lower peak value than the one before, what seems logical if the inlet velocity tends to decrease. The first maximum peak appears in agreement with the maximum inlet velocity.

The pressure, velocity and vorticity profiles for different states of the valve movement cycle are shown in Figure 4, whereas Figure 5 depicts the pressure profiles along the valve reed. The flow phenomena observed is consistent with previous studies [4] and accomplishes a qualitative accurate transient simulation of the turbulent flow. In agreement with the sudden increment of the inlet velocity according to the piston based inlet condition, a considerable increase of velocity is appreciated in the valve aperture when it starts to open. Hence, huge velocity gradients and consequently high vorticity appear in this area, where the mesh should be particularly fine to capture the smallest scales of the flow. Referring to this, the RBF method allows that the mesh quality is maintained in this region, provided that the initial mesh has sufficient number of CVs below the valve plate and the parameter radius of the RBF interpolation is chosen appropriately. Therefore, the CFD and dynamic mesh coupled code TermoFluids would be capable to carry out successfully the transient simulation of the flow through the suction reed valve, even with more complex geometries.

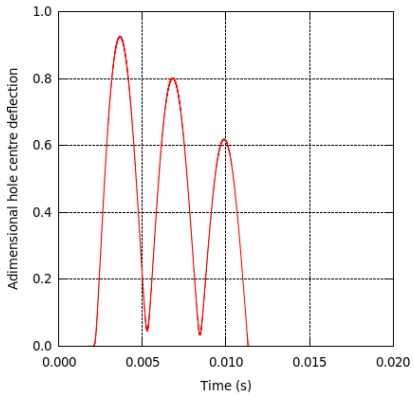

Figure 3: Hole centre deflection history during a valve cycle.

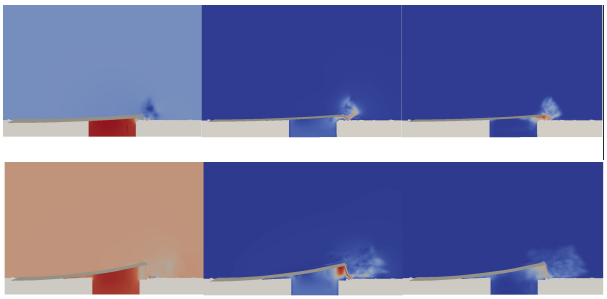

Figure 4: Pressure (left), velocity (middle) and vorticity (right) profiles for two intermediate states of the valve opening cycle.

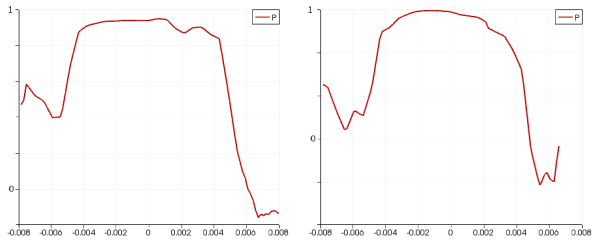

Figure 5: Adimensional pressure profile along the valve reed for the two intermediate states of the valve opening cycle in Figure 6, respectively.

REFERENCES

[1] W. Soedel. Mechanics, simulation and design of compressor valves, gas passages and pulsation mufflers. In *Purdue University Short Courses*. IN, USA, 1992.

[2] O. Lehmkuhl, R. Borrell, C. D. Perez-Segarra, M. Soria, and A. Oliva. TermoFluids: A new parallel unstructured CFD code for the simulation of turbulent industrial problems on low cost PC cluster. *Parallel Computational Fluid Dynamics 2007*, 67:275–282, 2009.

[3] O. Estruch, O. Lehmkuhl, R. Borrell, C. D. Perez-Segarra, and A. Oliva. A parallel radial basis function interpolation method for unstructured dynamic meshes. *Computer and Fluids*, 80:44–54, 2012.

[4] J. Rigola, O. Lehmkuhl, J. Ventosa, C. D. Perez-Segarra, and A. Oliva. Numerical simulation of the turbulent fluid flow through valves based on low mach models. *International Compressor Engineering Conference at Purdue University*, 60:116–134, 2011.

[5] F. X. Trias and O. Lehmkuhl. A self-adaptive strategy for the time integration of navier-stokes equations. *Numerical Heat Transfer, Part B: Fundamentals*, Indiana, USA, 2012.

[6] F. Nicoud and F. Ducros. Subgrid-scale stress modelling based on the square of the velocity gradient tensor. *Flow, Turbulence and Combustion*, 62:183–200, 1999.

LARGE EDDY SIMULATION OF A TURBULENT JET DIFFUSION FLAME USING UNSTRUCTURED MESHES

C.D. Pérez-Segarra[1], J. Ventosa[1], O. Lehmkuhl[1,2], A. Oliva[1]
[1] Centre Tecnològic de Transferencia de Calor, Universitat Politècnica de Catalunya, Spain
[2] Termo Fluids, S.L.

INTRODUCTION

In this work a turbulent jet diffusion flame, the DLR Flame A, is simulated numerically using Large Eddy Simulations (LES). This flame uses a mixture of $CH_4/H_2/N_2$ as fuel, has a Reynolds number of 15200 and presents a low level of local extinction. Three dimensional unstructured finite volume meshes are used to discretise the domain. Discretisation of the equations differential operators is performed by means of kinetic energy preserving schemes. Closure for the momentum turbulent stresses is performed by means of the QR subgrid scales (sgs) model. The chemistry-turbulence interactions are modelled using the Flamelet/Progress variable model [6], as it is capable of representing the whole range of states from ignition to extinction. Differential diffusion effects are taken into account when constructing the flamelet libraries.

Flamelet based models assume that chemical kinetics are much faster than mixing processes and that there exists universal flame structures at the smallest scales. In this context, a good resolution of the flow structures and scalars transport is critical to the correct prediction of combustion processes, specially in mixing controlled regimes. Conservative discretisations for the momentum equations, which as preserve kinetic energy by formulation, are shown to yield accurate results.

DESCRIPTION OF NUMERICAL METHOD

Flow Model. The flow here considered presents a low Mach number and high density variations, so the Low Mach Number approximation to the Navier Stokes is here considered, in terms of Favre-filtered quantities

$$\frac{\partial \overline{\rho}}{\partial t} + \mathbf{M}\widetilde{u} = 0 \tag{1}$$

$$\frac{\partial \overline{\rho}\widetilde{u}}{\partial t} = -\mathbf{C}(\overline{\rho}\widetilde{u})\widetilde{u} + (\mathbf{D} + \mathbf{D}_{tu})\widetilde{u} + \mathbf{G}\overline{p} + \overline{\rho}g \tag{2}$$

$$\overline{\rho}\frac{\partial \widetilde{f}}{\partial t} = -\overline{\rho}\mathbf{C}(\widetilde{u})\widetilde{f} + (\mathbf{D} + \mathbf{D}_{t,f})\widetilde{f} \tag{3}$$

$$\overline{\rho}\frac{\partial \widetilde{c}}{\partial t} = -\overline{\rho}\mathbf{C}(\widetilde{u})\widetilde{c} + (\mathbf{D} + \mathbf{D}_{t,c})\widetilde{c} + \widetilde{\dot{w}}_c \tag{4}$$

where $\mathbf{C}(\overline{\rho}\widetilde{u})$ and $\overline{\rho}\mathbf{C}(\widetilde{u})$ represent the conservative and non-conservative form of the convective operator, $\mathbf{D}$ represents the diffusive operator and $\mathbf{D}_{t,u}$ and $\mathbf{D}_{t,\phi}$ represent the modelled turbulent fluxes, $\mathbf{G}$ is the gradient operator and $\mathbf{M}$ is the mass divergence operator.

In order to close the momentum turbulent transport term, $\mathbf{D}_{t,u}$, the QR [1] SGS model is employed. Closure for the turbulent scalar-diffusivity $\alpha_{t,\phi} = C_\phi \Delta^2 |\widetilde{S}|$ is performed by a dynamic procedure as performed by Pierce and Moin [2], being S the strain tensor and Δ representing the LES filter width. A unity Lewis number assumption is used for the molecular diffusivities.

The mixture fraction variance is computed assuming local homogeneity and local equilibrium for the subgrid scales, then, an algebraic model is used to relate the subgrid variance of a conserved scalar to the gradients of the resolved scalar field

$$\overline{\rho}\widetilde{f''^2} = C_v \Delta^2 \overline{\rho} |\nabla \widetilde{f}|^2 \tag{5}$$

where C_v is calculated using the dynamic "LED" procedure of Balarac [3]. For the dynamic evaluation of both turbulent scalar-diffusivity and subgrid variance a top-hat test filter is used, created by face connectivity, due to the use of unstructured meshes.

The temporal integration is performed by means of a 2nd order two-step prediction-corrector scheme as shown in [4].

Focus on the preservation of the differential operators' properties is placed on the numerical discretisation schemes used for the momentum equations. For this reason the Symmetry Preserving scheme proposed by Verstappen [5] is used to discretise the convective operator and a 2nd order central difference is used to discretise the diffusive operator.

Combustion Model. A flamelet/progress-variable approach [6] is used in this work, which assumes that chemical reactions take place in thin one dimensional sheets known as flamelets. As shown in [7], solution of these one dimensional flamelets can be expressed as a state relation. Favre-filtered quantities are recovered from the flamelet solutions assuming the statistical distributions. Statistical independence between mixture fraction and the progress-variable is assumed. Additionally, a β-pdf is assumed for the mixture fraction and a δ-pdf is used for the progress-variable. The state relation is then

$$\widetilde{\phi} = \widetilde{F}_\phi(\widetilde{f}, \widetilde{f''^2}, \widetilde{c}) \tag{6}$$

STUDY CASE

The case of study is the axisymmetric jet flame known as DLR Flame A [8, 9]. It consists of a $D = 8mm$ wide jet with a thinned rim at the exit. The inner jet is composed of 33.2% H_2, 22.1% CH_4, and 44.7% N_2 by volume and the outer jet is regular air with 20.1% O_2. The cold jet exit bulk velocity is fixed to $42.15m/s$ resulting in a Reynolds number of $15,200$. The jet was mounted concentrically to the coflow nozzle, which had a diameter of $140mm$ and provided air at $0.3m/s$. Both fuel and coflow air were at $300K$.

RESULTS

Time-averaged results using the meshes of 250,000CV and 1.8MCV are compared against the experimental data [8, 9]. Fig. 1 and 2 show the radial profiles of the mixture fraction intensities and the axial velocity intensities respectively. Good agreement is found between numerical computations and the experimental data. However, the mixture fraction variance is seen to be underpredicted at positions higher than $y/D = 10$. Nonetheless, the models are seen to correctly capture the flow behaviour using low order numerical schemes.

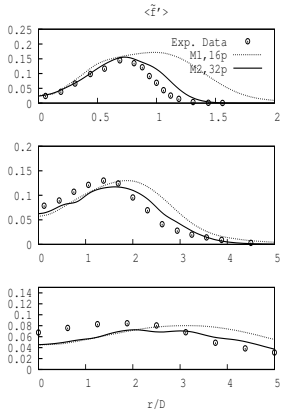

Figure 1: Radial distribution of the mixture fraction intensities. Top $y/D = 5$, middle $y/D = 20$, bottom $y/D = 40$.

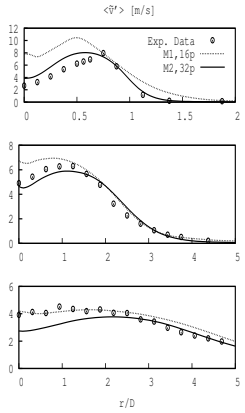

Figure 2: Radial distribution of the axial velocity intensities. Top $y/D = 5$, middle $y/D = 20$, bottom $y/D = 40$.

Figure 3 shows an instantaneous snapshot of the CO mass fraction. It can be seen that chemical reactions take place in thin regions of the flow and then the resulting species are transported downstream. It is also worth of note that near the nozzle there is a laminar region where differential diffusion effects are noticeable.

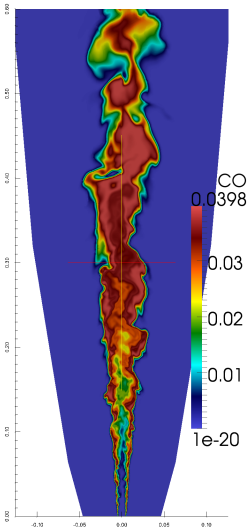

Figure 3: Snapshot of the instantaneous Y_{CO} field. The vertical axis is in $[m]$ and $0.6m \equiv 75y/D$

REFERENCES

[1] Verstappen, R. (2010) When does eddy viscosity damp subfilter scales sufficiently? *Quality and Reliability of Large-Eddy Simulations II, volume 16 of Ercoftac Series*, vol. 16, pp. 421–430, M.V. Salvetti, B. Geurts, J. Meyers, and P. Sagaut, editors.

[2] Pierce, C. and Moin, P. (1998) A dynamic model for subgrid-scale variance and dissipation rate of a conserved scalar. **10**, 3041.

[3] Balarac, G., Pitsch, H., and Raman, V. (2008) Development of a dynamic model for the subfilter scalar variance using the concept of optimal estimators. **20**, 035114.

[4] Ventosa, J., Chiva, J., Lehmkuhl, O., Pérez-Segarra, C., and Oliva, A. (2012) Low mach navier-stokes equations on unstructured meshes. *Proceedings of the The 15th International Conference on Fluid Flow Technologies*.

[5] Verstappen, R. and Veldman, A. (2003) Symmetry-preserving discretization of turbulent flow. **187**, 343–368.

[6] Pierce, C. and Moin, P. (2004) Progress-variable approach for large-eddy simulation of non-premixed turbulent combustion. **504**, 73–97.

[7] Ventosa, J., Lehmkuhl, O., Pérez-Segarra, C., and Oliva, A. (2013) Large eddy simulation of a turbulent jet diffusion flame using the flamelet-progress variable model. *Proceedings of the 6th European Combustion Meeting*.

[8] Meier, W., Barlow, R., Chen, Y.-L., and Chen, J.-Y. (2000) Raman/Rayleigh/LIF measurements in a turbulent CH4/H2/N2 jet diffusion flame: Experimental techniques and turbulencechemistry interaction. **123**, 326–343.

[9] Bergmann, V., Meier, W., Wolff, D., and Stricker, W. (1998) Application of spontaneous Raman and Rayleigh scattering and 2D LIF for the characterization of a turbulent CH4/H2/N2 jet diffusion flame. **66**, 489–502.

Variational multiscale large eddy simulation of turbulent incompressible flows.

O. Colomés[1] S. Badia[1,2], R. Codina[1,2] and J. Principe[1,2]

[1] International Center for Numerical Methods in Engineering (CIMNE)
Gran Capitán s/n, 08034, Barcelona, Spain
{badia,codina,colomes,principe}@cimne.upc.edu

[2] Universitat Politècnica de Catalunya
Jordi Girona 1-3, Edifici C1, 08034, Barcelona, Spain

The variational multiscale (VMS) method was introduced in [4] as a framework for the development of stabilization techniques, which aim to overcome numerical difficulties encountered when using the standard Galerkin method, the finite element (FE) counterpart of centered finite differences (FD), namely, the compatibility condition between the velocity and pressure FE spaces, which require the use of staggered grid in the FD context, and the nonphysical oscillations the could appear in the convection dominated regime, when the mesh is not fine enough.

The VMS method was then used proposed as an implicit large eddy simulation (LES) technique in [5] although in these early approaches small scales were explicitly solved introducing a Smagorinsky-type dissipative term. As a result, an important fraction of the degrees of freedom are used for the small resolved scales whereas consistency is retained in the large resolved scales only. ILES using a VMS approach with a resolved and a modeled subgrid scale (the setting that permits to recover stabilized formulations) was suggested in [2] and excellent numerical results were obtained in [1]. Compared to explicit LES, the VMS approach does not face difficulties associated with inhomogeneous non-commutative filters in wall-bounded flows and retains numerical consistency in the FE equations up to the interpolation order whereas e.g. the Smagorinsky model introduces a consistency error of order $h^{4/3}$.

The dissipative structure of variational multiscale methods has been analyzed in [6] where it is compared to the physical based LES dissipative structure. Simple LES closures (e.g. Smagorinsky) that could be used as an engineering design tool are purely dissipative whereas VMS methods can predict more complex energy transfers. The way the energy is exchanged between coarse and fine scales depends on the approximation performed on the fine scale equation. Dynamic and orthogonal subgrid scales introduced in [2, 3] result in a formulation with important numerical properties such as commutativity of space and time discretization or global conservation statements and a dissipative structure that presents the correct behavior in the laminar limit and is able to predict backscatter.

Apart from a discussion of these properties, we present detailed numerical results of the simulation of the decay of homogeneous isotropic turbulence. We study the influence of the different subgrid possibilities, the influence of the algorithmic constants in the stabilization parameters and the computational costs of different approaches. Finally, we compare the results obtained using VMS models against those obtained using classical LES based on filtering and the Smagorinsky closure. We do so using the Galerkin approximation of the Navier Stokes equations with a Taylor-Hood Q2/Q1 interpolation which satisfies the inf-sup condition, relying on the Smagorinsky term to stabilize convection.

References

[1] Y. Bazilevs, V.M. Calo, J.A. Cottrell, T. J. R. Hughes, A. Reali, and G. Scovazzi. Variational multiscale residual-based turbulence modeling for large eddy simulation of incompressible flows. *Comp. Meth. App. Mech. Eng.*, 197(1-4):173–201, 2007.

[2] R. Codina. Stabilized finite element approximation of transient incompressible flows using orthogonal subscales. *Comp. Meth. App. Mech. Eng.*, 191(39-40):4295–4321, Aug 2002.

[3] R. Codina, J Principe, O Guasch, and S Badia. Time dependent subscales in the stabilized finite element approximation of incompressible flow problems. *Comp. Meth. App. Mech. Eng.*, 196(21-24):2413–2430, 2007.

[4] T. J. R. Hughes, G. R. Feijóo, L. Mazzei, and J.B. Quincy. The variational multiscale method–a paradigm for computational mechanics. *Computer Methods in Applied Mechanics and Engineering*, 166:3–24, 1998.

[5] T. J. R. Hughes, L. Mazzei, and K. E. Jansen. Large eddy simulation and the variational multiscale method. *Computing and Visualization in Science*, 3:47–59, 2000.

[6] J. Principe, R. Codina, and F. Henke. The dissipative structure of variational multiscale methods for incompressible flows. *Comp. Meth. App. Mech. Eng.*, 199:791–801, 2010.

Variational multiscale large eddy simulation of turbulent thermally coupled flows.

M. Ávila[3], R. Codina[1,2], and J. Principe[1,2]

[1] International Center for Numerical Methods in Engineering (CIMNE)
Gran Capitán s/n, 08034, Barcelona, Spain
{badia,codina,colomes,principe}@cimne.upc.edu

[2] Universitat Politècnica de Catalunya
Jordi Girona 1-3, Edifici C1, 08034, Barcelona, Spain

[3] Barcelona Supercomputing Center
Gran Capitán 2-4, 08034, Barcelona, Spain
matias.avila@bsc.es

Residual based variational multiscale methods (VMM) for turbulence modeling have proven to give very good results for fully developed and transitional turbulent flows [2]. This approach contrasts to the classical LES models based on filtering (e.g. Smagorinsky) which introduce a physical dissipation at the continuous level.

The main difference is precisely the way in which resolved and subgrid scales are defined. The use of filtering as splitting mechanism gives rise to important difficulties and a degrading of the convergence rate [2]. By contrast, VMM modeling is based on a projection splitting and the approximation of the subgrid problem, which results in an optimally convergent method.

In this talk we present a VMS finite element approximation of thermally coupled low speed flows[1]. The physical model is described by the low Mach number equa- tions, which are obtained as a limit of the compressible NavierStokes equations in the small Mach number regime. In contrast to the commonly used Boussinesq approximation, this model permits to take volumetric deformation into account. Although the former is more general than the latter, both systems have similar mathematical structure and their numerical approximation can suffer from the same type of instabilities.

Using this approach we study the approximation to thermal turbulence from a strictly numerical point of view, without the use of any turbulence model. The main goal is to analyze the behavior of our numerical method in the simulation of thermally coupled turbulent flows at low Mach number. Our numerical method is a stabilized finite element approximation based on the VMS method, in which a decomposition of the approximating space into a coarse scale resolvable part and a fine scale subgrid part is performed. Modeling the subscale and taking its effect on the coarse scale problem into account results in a stable formulation. The quality of the final approxima- tion (accuracy, efficiency as turbulent numerical model) depends on the particular subscale model. The distinctive features of our approach are to consider the subscales as transient and to keep the scale splitting in all the nonlinear terms [3, 4].

Apart from a laminar testcase validation, we present results of the numerical simulation of the turbulent channel flow with large temperature differences in the normal direction, a classical benchmark problem. The Reynolds number is 180 based on the channel half height and the mean friction velocity. The behavior of the method is evaluated by comparison against results available in the literature obtained using a classical Large Eddy Simulation (LES). The behavior of the method is evaluated by comparison against results available in the literature obtained using a direct numerical simulation (DNS). Besides, they are explained based on a careful analysis of the dissipative structure of the method, showing the physical interpretation of the subgrid scale method presented, as an extension of the results for incompressible flows obtained in [5].

References

[1] M. Avila, J. Principe, and R. Codina. A finite element dynamical nonlinear subscale approximation for the low mach number flow equations. *Journal of Computational Physics*, 230(10-11):7988–8009, 2011.

[2] Y. Bazilevs, V.M. Calo, J.A. Cottrell, T. J. R. Hughes, A. Reali, and G. Scovazzi. Variational multiscale residual-based turbulence modeling for large eddy simulation of incompressible flows. *Comp. Meth. App. Mech. Eng.*, 197(1-4):173–201, 2007.

[3] R. Codina. Stabilized finite element approximation of transient incompressible flows using orthogonal subscales. *Comp. Meth. App. Mech. Eng.*, 191(39-40):4295–4321, Aug 2002.

[4] R. Codina, J Principe, O Guasch, and S Badia. Time dependent subscales in the stabilized finite element approximation of incompressible flow problems. *Comp. Meth. App. Mech. Eng.*, 196(21-24):2413–2430, 2007.

[5] J. Principe, R. Codina, and F. Henke. The dissipative structure of variational multiscale methods for incompressible flows. *Comp. Meth. App. Mech. Eng.*, 199:791–801, 2010.